Electronic Supplementary Material (ESI) for Physical Chemistry Chemical Physics.
This journal is © the Owner Societies 2019

Electronic Supplementary Information (ESI) for

The dual-defected SnS_2 monolayers: Promising 2D photocatalysts for overall water splitting

Batjargal Sainbileg, [ab] Ying-Ren Lai, [abc] Li-Chyong Chen [ab] and Michitoshi Hayashi*[ab]

[a]Center for Condensed Matter Sciences, National Taiwan University, Taipei 106, Taiwan

[b]Center of Atomic Initiative for New Materials, National Taiwan University, Taipei 106, Taiwan

[c]Department of Chemistry, National Taiwan University, Taipei 106, Taiwan

Corresponding Author E-mail: atmyh@ntu.edu.tw

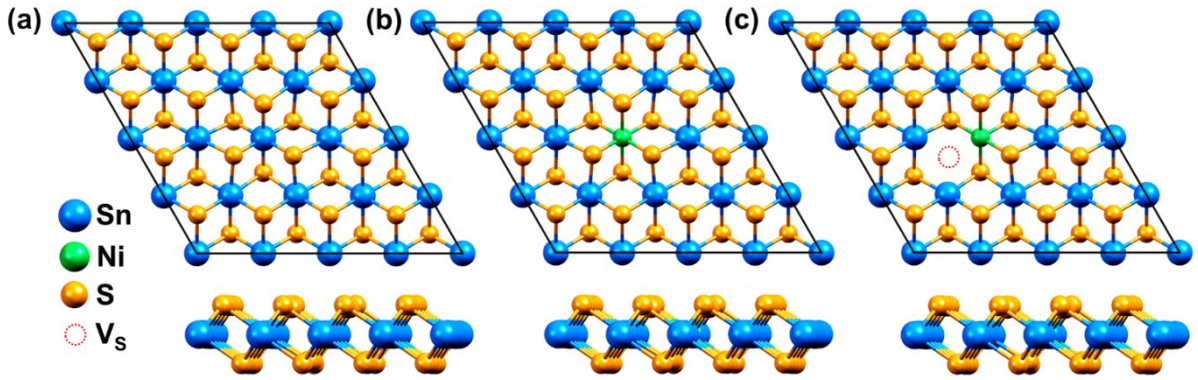

Fig. S1. Structure of (a) pristine SnS_2, (b) Nickel doped SnS_2 (Ni-SnS_2) and (c) Nickel doped SnS_2 with sulfur monovacancy defect (Ni-SnS_2-V_S). The black box illustrates the periodic supercell while the blue, yellow and green spheres represent the tin, sulfur and nickel atoms, respectively.

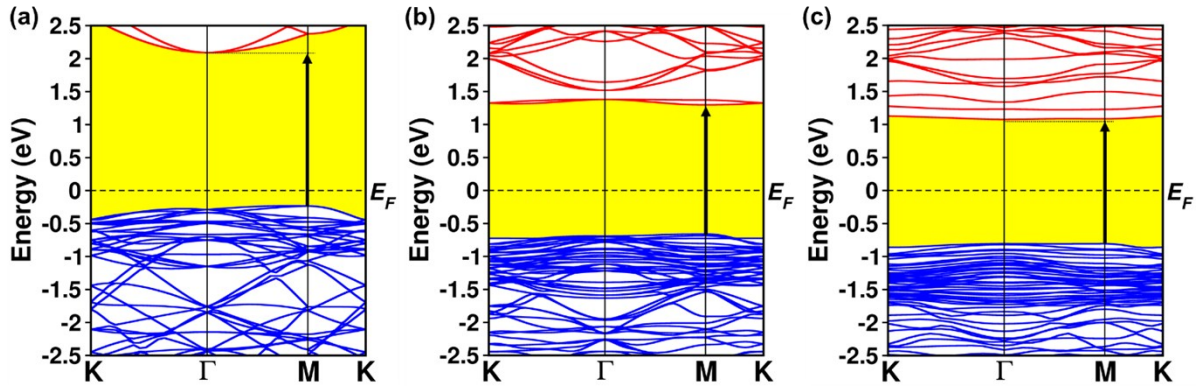

Fig. S4. Band structures of (a) pristine SnS_2, and defective (b) Ni-SnS_2 and (c) Ni-SnS_2-V_S. The red and blue lines represent the conduction and valence bands, respectively, whereas the dashed line illustrates the Fermi level E_F. The band structure of SnS_2 and Ni-SnS_2 are adapted with permission from our recent work in the ref [1]. Copyright (2019) Chemical Physics.

Table S1. The formation energy of the investigated SnS_2 monolayers relative to pure SnS_2

Monolayer structures	Relative formation energy (eV)
Pristine SnS_2	0
Ni-SnS_2	1.10
Ni-SnS_2-Vs	1.96

Note that all formation energy refers to the hereafter is relative formation energy compared with the pristine SnS_2.

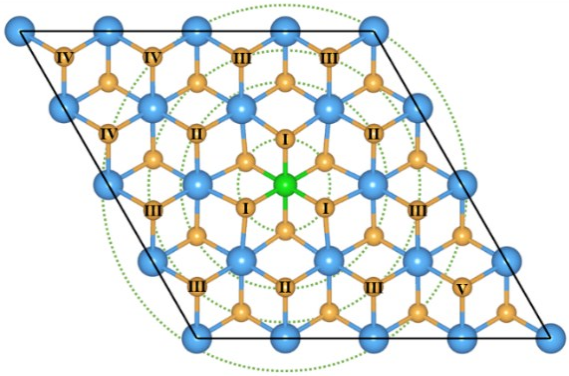

Fig. S2. Possible positions of sulfur monovacancy in the Ni-SnS_2 monolayers have been tested.

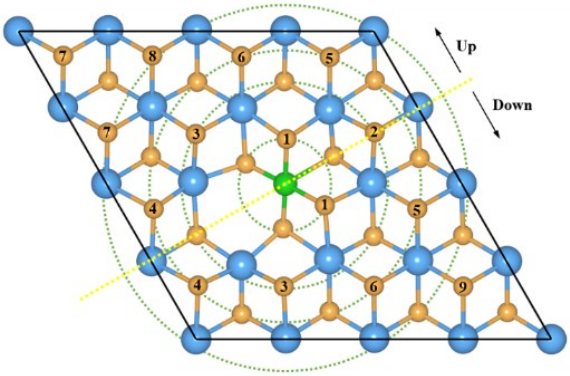

Fig. S3. Possible positions of two- and three-sulfur vacancies in the Ni-SnS_2-V_{NS} monolayers have been tested.

Table S2. The relative formation energy of the Ni-SnS_2-V_S monolayers with different positions of sulfur monovacancy regarding a nickel dopant

The first S-vacancy location	Distance (V_S-Ni) (Å)	Formation energy (eV)
Ni-SnS_2-V_S (I)	2.34	1.96
Ni-SnS_2-V_S (II)	4..53	2.74
Ni-SnS_2-V_S (III)	5.82	2.74
Ni-SnS_2-V_S (IV)	7.84	2.67
Ni-SnS_2-V_S (V)	8.67	3.12

Table S3. The relative formation energy of the Ni-SnS_2-V_{2S} monolayers with different positions of two sulfur vacancies regarding a nickel dopant (see Fig. S3)

The second S-vacancy location	Distance (V_S-Ni) (Å)	Formation energy (eV)
Ni-SnS_2-V_{2S} (1)	2.26	3.37
Ni-SnS_2-V_{2S} (2)	4.49	3.34
Ni-SnS_2-V_{2S} (3)	4.49	3.07
Ni-SnS_2-V_{2S} (4)	5.71	3.02
Ni-SnS_2-V_{2S} (5)	5.73	3.32
Ni-SnS_2-V_{2S} (6)	5.78	3.64
Ni-SnS_2-V_{2S} (7)	7.79	3.42
Ni-SnS_2-V_{2S} (8)	7.80	3.88
Ni-SnS_2-V_{2S} (9)	8.61	3.43

Table S4. The relative formation energy of the Ni-SnS_2-V_{3S} monolayers with different positions of three sulfur vacancies regarding a nickel dopant (see Fig. S3)

The second and third S-vacancy location	Formation energy (eV)
Ni-SnS_2-V_{3S} (2,6)	4.89
Ni-SnS_2-V_{3S} (3^d,4^d)	4.14
Ni-SnS_2-V_{3S} (4^u,4^d)	4.78
Ni-SnS_2-V_{3S} (3^u,4^d)	4.24
Ni-SnS_2-V_{3S} (3^u,3^d)	4.28
Ni-SnS_2-V_{3S} (2,4^d)	4.22

Here, “u” and “d” are abbreviations of up and down (see Fig. S3).

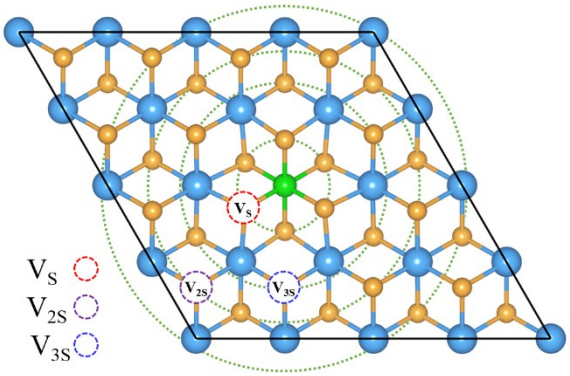

Fig. S5. Selected positions of the sulfur vacancies in the Ni-SnS_2-V_{NS} monolayer owing to more favorable formation energy.

Table S5. The relative formation energy of the more favorable configurations among the all tested Ni-SnS_2-V_{NS} monolayers

Selected Ni-SnS_2-V_{NS}	Formation energy (eV)
Ni-SnS_2-V_S	1.96
Ni-SnS_2-V_{2S}	3.02
Ni-SnS_2-V_{3S}	4.14

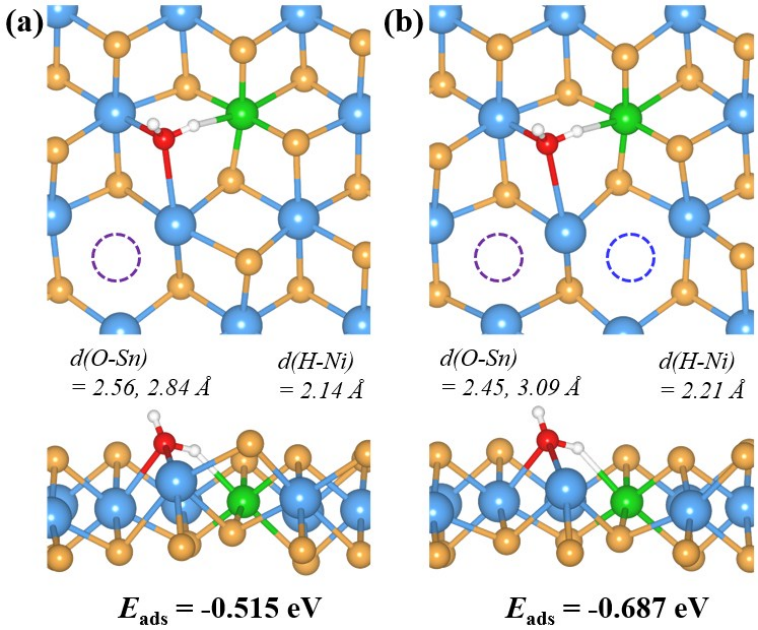

Fig. S6. Water adsorption on (a) Ni-SnS_2-V_{2S} and (b) Ni-SnS_2-V_{3S} monolayer. Note that the E_{ads} of H_2O on the Ni-SnS_2-V_{2S} and Ni-SnS_2-V_{3S} are still high, showing chemisorption of an H_2O molecule. However, E_{ads} values of the Ni-SnS_2-V_{2S} and Ni-SnS_2-V_{3S} are lower than -0.879 eV on Ni-SnS_2-V_S.

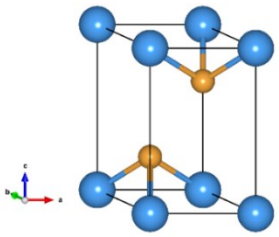

Fig. S7. The unit cell of bulk SnS_2, being a 2H polytype, has the hexagonal structure with *P-3m1* symmetry (space group 164) and lattice constants of $a = b = 3.65$ Å and $c = 5.89$ Å [2], adopting as initial crystal structure. After optimization calculation with the DFT-D3 method, the optimized unit cell of SnS_2 had the lattice constants of $a = b = 3.67$ Å, $c = 5.90$ Å, $\alpha = \beta = 90°$, and $\gamma = 120°$, which are consistent with previous experimental results [3-5], whereas the optimized SnS_2 monolayer has the 4×4×1 supercell with lattice constants of $a = b = 14.7$ Å and $c = 25.0$ Å.

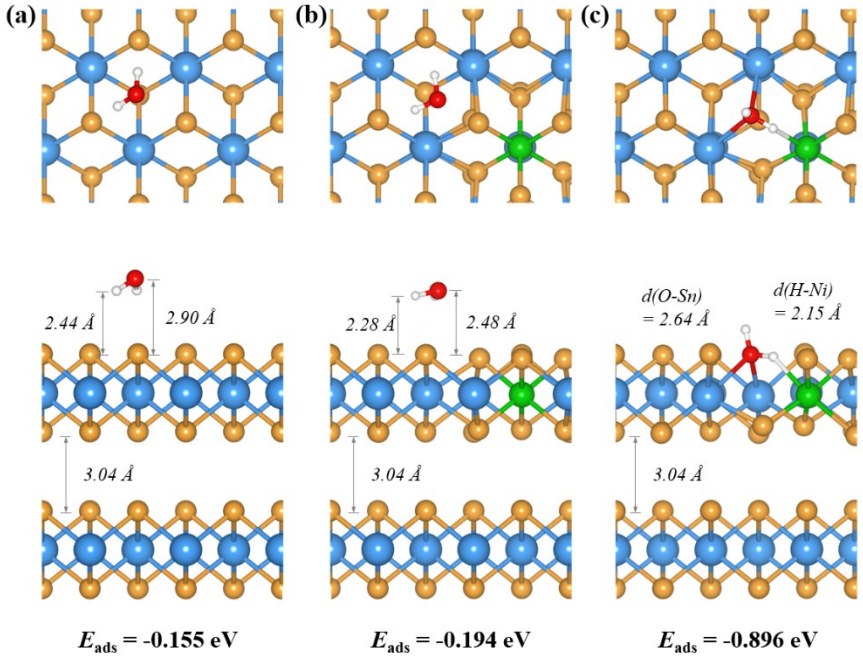

Fig. S8. Water adsorption on (a) SnS_2 (b) Ni-SnS_2 and (c) Ni-SnS_2-V_S bilayers. E_{ads} of an H_2O on pristine SnS_2 and Ni-SnS_2 bilayers do not show an obvious discrepancy from that of their monolayers while the E_{ads} for dual-defected bilayer is increased by 0.017 eV only (see also Table S6).

Table S6. Comparison for E_{ads} of an H_2O on mono- and bilayers of SnS_2, Ni-SnS_2, Ni-SnS_2-V_S

SnS_2 structures	E_{ads} at monolayer (eV)	E_{ads} at bilayer (eV)	Difference (eV)
Pristine SnS_2	-0.154	-0.155	-0.001
Ni-SnS_2	-0.189	-0.194	-0.005
Ni-SnS_2-V_S	-0.879	-0.896	-0.017

The COHP and iCOHP of the most stable water adsorption configurations on pure SnS_2, Ni-SnS_2 and Ni-SnS_2-V_S monolayers

To understand the interaction between the H_2O molecule and surfaces, we have generated the COHP (crystal orbital Hamilton population) and iCOHP (integrated crystal orbital Hamilton population) values by using the LOBSTER program[3]. The COHP and iCOHP plots are presented in Fig. S9-S12 where the positive (negative) COHP values indicate bonding (antibonding) contributions between two selected atoms whereas the positive iCOHP values represents the net bonding contributions to the pair.

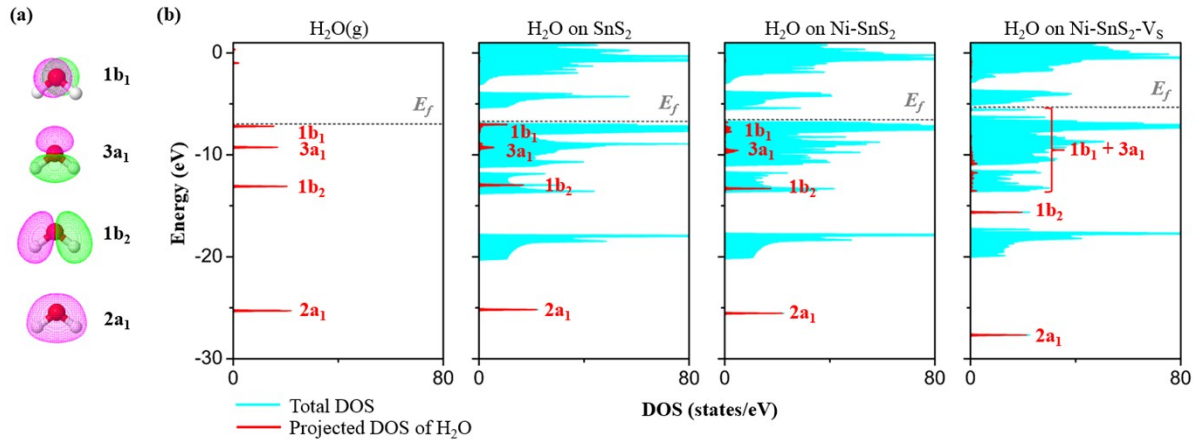

Fig. S9. (a) Occupied valence orbitals of the gas phase H_2O molecule. (b) DOS plots for the H_2O molecule absorption on SnS_2, Ni-SnS_2 and Ni-SnS_2-V_S monolayers. For comparison, all energies are referred to as $E_{(\text{vacuum-potential})} = 0$. From these projected DOS of the H_2O molecule, we can find that the H_2O molecule interacted with these surfaces predominantly through the $1b_1$ (lone pair) and $3a_1$ orbitals. The stronger interaction between the H_2O molecule and the Ni-SnS_2-V_S monolayer results in the much broadening of $1b_1$ and $3a_1$ peaks.

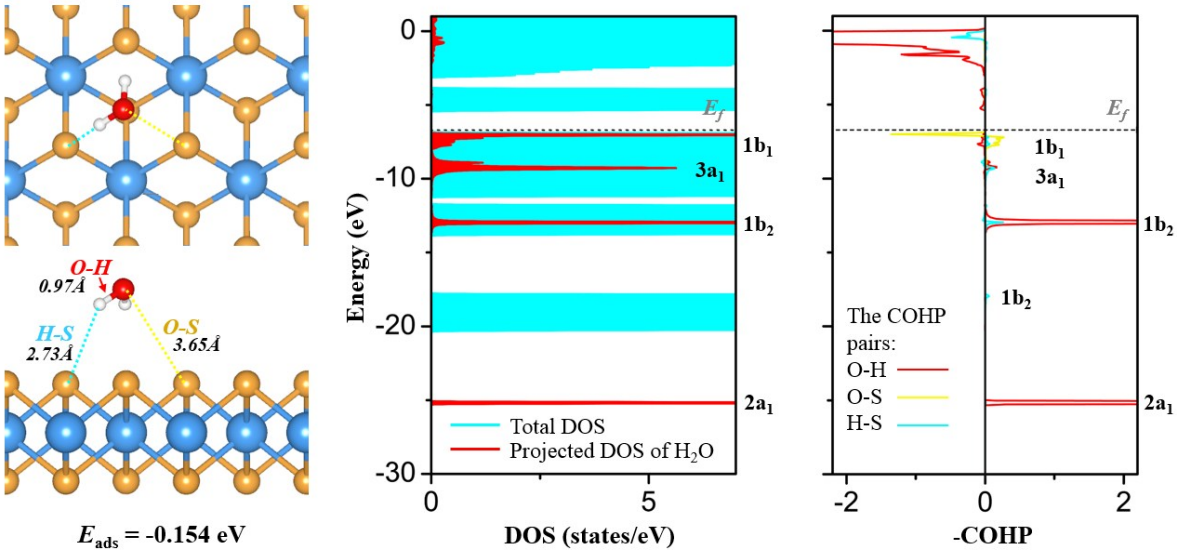

Fig. S10. The relevant bond distance, DOS and COHP plots of the most stable H_2O molecule adsorption configuration on the pure SnS_2 monolayer. The iCOHP value for the O-H bond (indicated in the red arrow) is +7.262 and this is slightly weaker than the iCOHP value for the O-H bond of the gas phase H_2O (+7.410 from our calculation). The iCOHP value for the O-S bond (indicated in the yellow dot line) is +0.015 and for the H-S (indicated in the blue dot line) bond is +0.107. These two interactions are weak and include bonding and antibonding interactions as shown in the COHP plot. Notably, the interactions between the O atom of the H_2O molecule and the surface S atom are mainly due to the lone pair interactions, which include the similar magnitude of bonding and antibonding interactions and sum to a small iCOHP value.

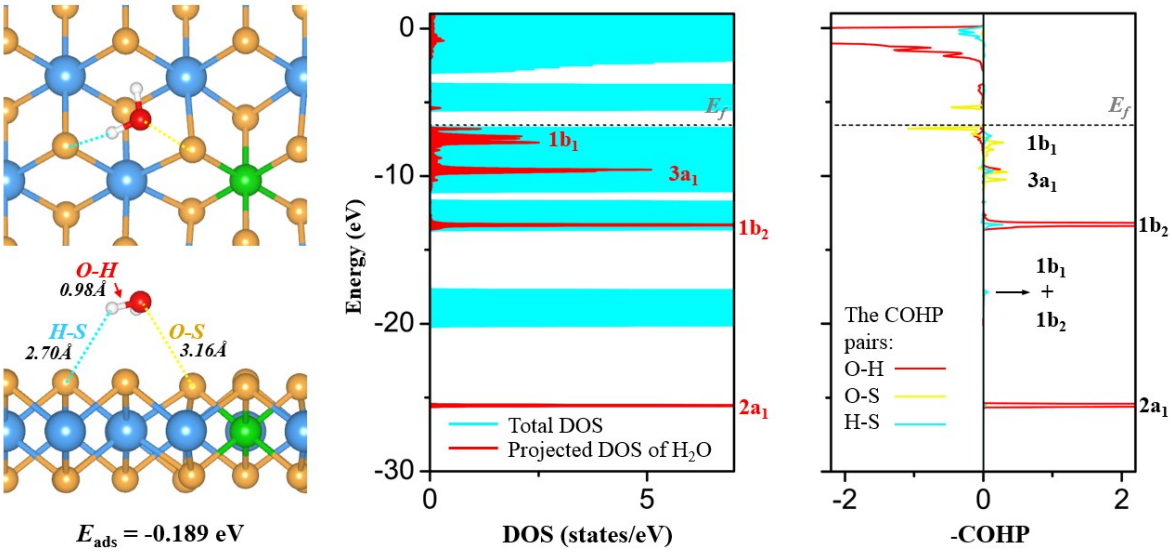

Fig. S11. The relevant bond distance, DOS and COHP plots of the most stable H_2O molecule adsorption configuration on Ni-SnS_2 monolayer. The iCOHP value for the O-H bond (indicated in the red arrow) is +7.343 and this is slightly weaker than the iCOHP value for the O-H bond of the gas phase H_2O (+7.410). The iCOHP value for the O-S bond (indicated in the yellow dot line) is +0.068 and for the H-S (indicated in the blue dot line) bond is +0.130. After Ni-doping, the lone pair repulsion between the $1b_2$ molecular orbital of the H_2O molecule and the *p*-orbitals of the surface S atom is slightly reduced and new bonding interactions are formed between the $1b_2$ and $3a_1$ orbitals of the H_2O molecule and the *p*-orbitals of the surface S atom (near the range of -10 eV). The small increases of the iCOHP value of the O-S bond (about 0.053) and the H-S bond (about 0.023) match with the adsorption energy going from -0.154 eV to -0.189 eV with comparing to the results of the H_2O molecule adsorption on the pure SnS_2 monolayer in **Fig. S10**.

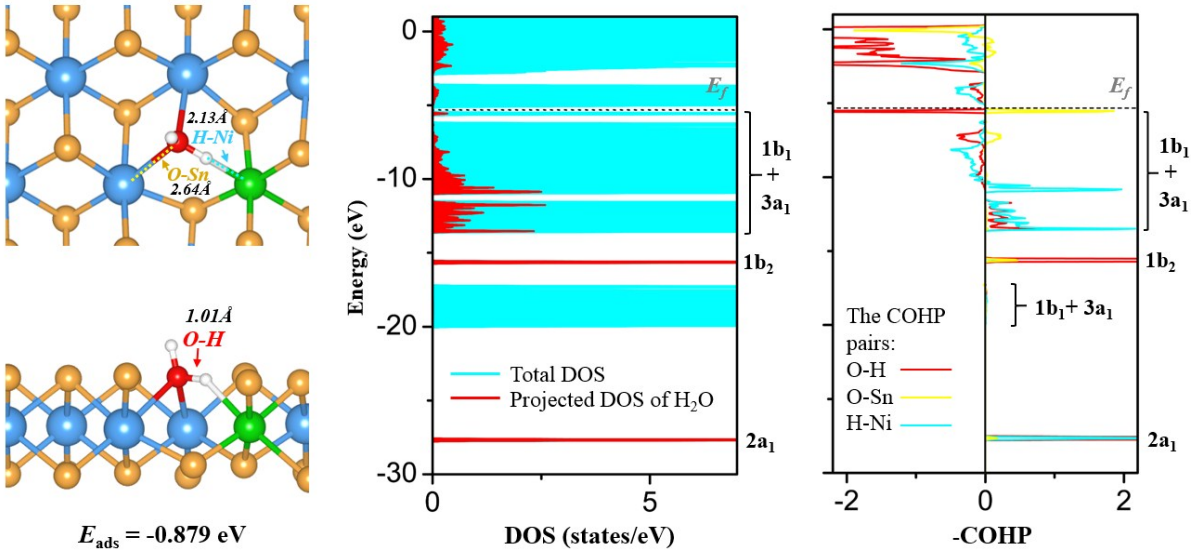

Fig. S12. The relevant bond distance, DOS and COHP plots of the most stable H_2O molecule adsorption configuration on the Ni-SnS_2-V_S monolayer. For this water chemisorption result, the O-H bond near the surface lengthens from 0.97 to 1.01 Å (indicated in the red arrow) and the corresponding iCOHP value decreases from +7.410 to +6.979. The weakening of this O-H bond is reflected in the antibonding contributions in the COHP plot (red line). The iCOHP value for the O-Sn bond (indicated in the yellow dot line) is +1.016 and for the H-Ni (indicated in the blue dot line) bond is +0.430.

REFERENCES

[1] B. Sainbileg and M. Hayashi, *Chem. Phys.*, 2019, **522**, 59–64.

[2] L. A. Burton, T. J. Whittles, D. Hesp, W. M. Linhart, J. M. Skelton, B. Hou, R. F. Webster, G. O'Dowd, C. Reece, D. Cherns, D. J. Fermin, T. D. Veal, V. R. Dhanak and A. Walsh, *J. Mater. Chem. A*, 2016, **4**, 1312–1318.

[3] Y. Sun, H. Cheng, S. Gao, Z. Sun, Q. Liu, Q. Liu, F. Lei, T. Yao, J. He, S. Wei and Y. Xie, *Angew. Chem. Int. Ed.*, 2012, **51**, 8727–8731.

[4] M. Ø. Filsø, E. Eikeland, J. Zhang, S. R. Madsen and B. B. Iversen, *Dalton Trans.*, 2016, **45**, 3798–3805.

[5] S. K. Arora, D. H. Patel and M. K. Agarwal, *Cryst. Res. Technol.*, 1993, **28**, 623–627.

[6] S. Maintz, V. L. Deringer, A. L. Tchougreeff and R. Dronskowski, *J. Comput. Chem.*, 2016, **37**, 1030–1035.